ON THE USE OF THE QUATERNION GENERALIZED GAUSSIAN DISTRIBUTION FOR FOOTSTEP DETECTION

Divya Venkatraman, Vinod V. Reddy and Andy W. H. Khong

Nanyang Technological University, Singapore
Email: divy0012@e.ntu.edu.sg, vinodreddy@pmail.ntu.edu.sg, andykhong@ntu.edu.sg

ABSTRACT

We propose a method to detect human footsteps from a vector-quaternion signal acquired by a tri-axial geophone. The quaternion generalized Gaussian distribution (QGGD) is derived to parameterize variations in the vector-quaternion signal using a shape parameter, quantifying non-Gaussianity and quaternion augmented covariance matrix, quantifying inter-channel correlation. The detection of footsteps is then formulated as binary hypotheses tests in terms of the parameters of the QGGD. The effectiveness of the proposed metrics is evaluated on recorded seismic data.

Index Terms— vector-sensor, quaternion, footstep detection.

1. INTRODUCTION

Seismic sensors are increasingly used in open-field surveillance systems to monitor human activity. Conventional human footstep detection methods include the use of single-axis geophones that employ either higher-order statistics such as kurtosis to quantify non-Gaussianity or cadence to quantify the periodicity of a train of footsteps [1]. The use of tri-axial geophones, with three orthogonally co-located sensors, have increased in recent years due to ease of deployment compared to multiple single-axis geophones. Such a vector-sensor has the inherent ability to detect 3-D particle velocity, which in turn, preserves the composite polarization characteristics of the impinging signal. Therefore, a single tri-axial geophone is able to exploit the fact that sources such as footsteps impacting the Earth's surface, generate waves that propagate predominantly as Love and Rayleigh modes giving rise to elliptical polarization [2].

Quaternions are hyper-complex numbers often used as a signal processing tool to express vector-sensor data [3]. In this work, we propose a novel technique that employs quaternion theories to model the diversity in the statistics of the data acquired from a single tri-axial geophone. To achieve footstep detection, a quaternion generalized distribution, which allows the analysis of both elliptically polarized footstep signal and unpolarized noise, is derived. The probability density function (pdf) of this quaternion generalized Gaussian distribution (QGGD) parameterizes variations in the vector-quaternion during the presence and absence of a polarized source, viz., human footsteps. As will be described, we model the peakyness of the multi-variate signal distribution using the shape parameter of the QGGD while the augmented covariance matrix of the QGGD is used to quantify the inter-channel correlation of the tri-axial geophone. We then formulate footstep detection as two binary hypothesis tests corresponding to the shape parameter and degree-of-$\mathbb{Q}$-improperness of the augmented covariance matrix.

2. RELATION TO PRIOR WORK

As opposed to existing footstep detection techniques that employ fourth-order statistics to quantify the peakyness and cadence to quantify the periodicity of footsteps [1], the novelty of this work lies in the use of quaternion distribution to quantify the dissimilarity in the statistics between footsteps and noise vector-quaternion signal. As will be shown, increasing source-sensor distance as well as multiple reflections from dispersive medium causes the spreading of and reduces the peakyness of footstep signature, resulting in poor detection performance of existing algorithms. However, we show that exploiting the interchannel correlation through the use of impropriety of the quaternion-valued signal results in improved detection of footstep signals. It is also important to note that real-world seismic signals cannot be completely described using existing Gaussian models [5] and hence we derive the quaternion generalized distribution as an extension of complex generalized distribution [6, 7]. The derived QGGD allows the modelling of wide variety of quaternion-valued random variables ranging from super-Gaussian, Gaussian to sub-Gaussian with different degrees of properness and hence can be extended to other applications such as oceanic studies using hydrophones [8]. The current work also differs from our earlier work [9] which quantified footstep signals using 3-D normalized velocity trajectory.

3. VECTOR-QUATERNION FOR FOOTSTEP SIGNALS

The signal acquired by a tri-axial geophone at any time instant n can be represented by a 3×1 column vector

$$\mathbf{x}(n) = [x_1(n) \;\; x_2(n) \;\; x_3(n)]^T, \tag{1}$$

where the first two elements define data corresponding to the two horizontal channels while the third element corresponds to the vertical channel. The three orthogonal channel data is well represented as a vector-quaternion

$$q_{\mathbf{x}}(n) = x_1(n)\imath + x_2(n)\jmath + x_3(n)\kappa, \tag{2}$$

where $\imath$, $\jmath$ and κ define the mutually orthogonal imaginary numbers such that $\imath^2 = \jmath^2 = \kappa^2 = -1$, $\imath\jmath = \kappa$, $\jmath\kappa = \imath$ and $\kappa\imath = \jmath$. The polar representation of $q_{\mathbf{x}}(n)$ is given by

$$q_{\mathbf{x}}(n) = \rho(n)e^{\zeta(n)\Theta(n)}, \tag{3}$$

where

$$\rho(n) = ||q_{\mathbf{x}}(n)||_2 = \sqrt{x_1^2(n) + x_2^2(n) + x_3^2(n)} \tag{4}$$

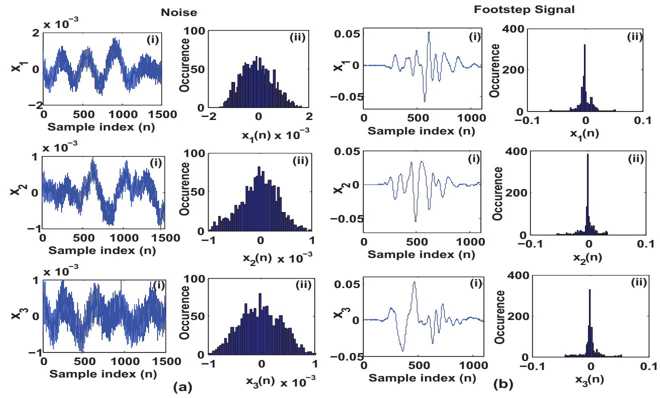

Fig. 1. Distribution of data - (i) data acquired from the tri-axial geophone and (ii) their distributions, for (a) noise (b) footstep segment.

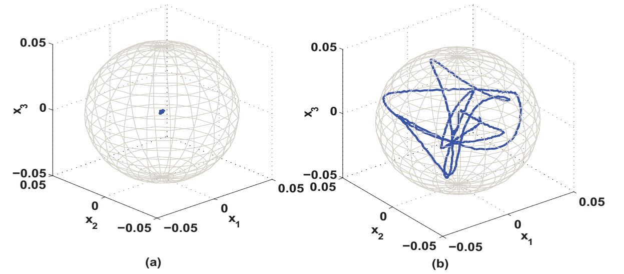

Fig. 2. 3-D plot of (a) noise-only and (b) footstep segment.

defines the magnitude, $\zeta(n) = q_{\mathbf{x}}(n)/||q_{\mathbf{x}}(n)||_2$ is the eigenaxis and $\Theta(n) = \pi/2$ is the eigenangle [3].

Figures 1 (a) and (b) illustrate the orthogonal components of the vector-quaternion signal for noise and a footstep, at a distance of 3 m from the sensor, respectively, along with their corresponding distributions. In the absence of a footstep, the distribution tends towards Gaussianity while in its presence, the distribution approaches super-Gaussianity. In addition, it has been described in [2] that footsteps generate multiple modes of polarization that is dominated by elliptically polarized Rayleigh waves. To illustrate the above, the time evolution of the signals shown in Fig. 1 is plotted in Fig. 2 using (1). As opposed to the absence of a footstep in Fig. 2(a), we note from Fig. 2(b) that the 3-D data in the presence of a footstep traces a wobbly orbit [10]. This elliptical polarization results in correlation between the three channel data of the geophone when a footstep is present. Along with this correlation, the difference in the signal distributions across orthogonal channels of the geophone, as observed in Fig. 1, gives rise to impropriety in the vector-quaternion signal, which is preserved in the quaternion augmented statistics. Thus the presence of a footstep is reflected both as super-Gaussianity in the individual axes as illustrated in Fig. 1, and as correlation between the axes of the vector-sensor as illustrated in Fig. 2. A vector-quaternion representation of tri-axial data retains the non-linear relation between the orthogonal components, as against long-vector [4] or component-wise processing. We therefore propose to derive and employ quaternion generalized Gaussian distribution (QGGD) with augmented statistics for footstep detection.

4. THE PROPOSED QUATERNION GENERALIZED GAUSSIAN DISTRIBUTION

We derive the pdf for the QGGD which parameterizes variations in the distribution pattern using a shape parameter and inter-channel correlation using quaternion augmented covariance matrix. Footstep detection can then be defined in terms of the parameters of this pdf. We first describe the quaternion augmented statistics needed for the derivation of the QGGD by defining the 4×1 quaternion augmented vector [11] as

$$\mathfrak{q}^{\mathrm{a}}_{\mathbf{x}}(n) = [q_{\mathbf{x}}(n) \;\; q^{\imath}_{\mathbf{x}}(n) \;\; q^{\jmath}_{\mathbf{x}}(n) \;\; q^{\kappa}_{\mathbf{x}}(n)]^T, \tag{5}$$

where $q^{\imath}_{\mathbf{x}}(n) = -\imath \star q_{\mathbf{x}}(n) \star \imath$ is known as the quaternion involution with respect to $\imath$, while $\star$ denotes the quaternion product. It is useful to note that quaternion involution with respect to $\imath$ defines a rotation by an angle π in the imaginary plane orthogonal to $\{1, \imath\}$. The corresponding quaternion augmented covariance matrix is evaluated as [11]

$$\mathbb{C}^{\mathrm{a}}_{\mathfrak{q}_{\mathbf{x}}} = \mathrm{E}\Big\{\mathfrak{q}^{\mathrm{a}}_{\mathbf{x}}(n)(\mathfrak{q}^{\mathrm{a}}_{\mathbf{x}})^H(n)\Big\}, \tag{6}$$

where $\mathrm{E}\{.\}$ and the superscript $(\cdot)^H$ are the expectation and Hermitian operators, respectively. The quaternion augmented covariance matrix $\mathbb{C}^{\mathrm{a}}_{\mathfrak{q}_{\mathbf{x}}}$ and the tri-variate covariance matrix evaluated as

$$\mathbb{C} = \mathrm{E}\Big\{\mathbf{x}(n)\mathbf{x}^T(n)\Big\}, \tag{7}$$

are related by the identity [11]

$$\mathbf{x}^T(n)\mathbb{C}^{-1}\mathbf{x}(n) = (\mathfrak{q}^{\mathrm{a}}_{\mathbf{x}})^H(n)(\mathbb{C}^{\mathrm{a}}_{\mathfrak{q}_{\mathbf{x}}})^{-1}\mathfrak{q}^{\mathrm{a}}_{\mathbf{x}}(n). \tag{8}$$

The variable $\mathbb{C}^{\mathrm{a}}_{\mathfrak{q}_{\mathbf{x}}}$ completely describes the second-order statistics of the vector-quaternion signal. With the above definitions we are ready to define the pdf for QGGD which is derived similar to its complex counterpart CGGD [6] by representing the vector-quaternion in its polar form using (3) with $\Theta(n) = \pi/2$.

We start the derivation by noting that the shape of the vector-quaternion distribution can be described by its magnitude $\rho(n)$ defined in (4). As described in [6], the magnitude of the CGGD is described by a modified Gamma variate and hence, in a similar manner, $\rho(n)$ is assumed to be a generalized Gamma distribution (GGaD) with shape parameters $(3/k, k)$ and unit scale, i.e., $\rho(n) \sim \mathrm{GGaD}(3/k, k, 1)$. The pdf of $\rho(n)$ is then given by [12]

$$p(\rho) = k\rho^2(n)e^{-\rho^k(n)}\Big/\Gamma(3/k), \tag{9}$$

where $\Gamma(3/k) = \int\limits_0^\infty e^{-t}t^{3/k-1}dt$ is the Gamma function.

Similarly extending on [6], the eigenaxis $\zeta(n)$ is assumed to be uniformly distributed on the surface of a sphere and described in terms of an azimuth angle $\chi(n) \sim \mathcal{U}(0, 2\pi)$ and elevation angle $\phi(n) \sim \mathcal{U}(0, \pi)$. Assuming $\rho(n)$, $\chi(n)$ and $\phi(n)$ are independent, the joint pdf (in polar form) is given by

$$p(\rho, \chi, \phi) = p(\rho)(1/2\pi)(1/\pi). \tag{10}$$

We note that the vector-quaternion can alternatively be expressed in terms of the Cartesian tri-variate random variables using $x_1(n) = \rho(n)\sin\phi(n)\cos\chi(n)$, $x_2(n) = \rho(n)\sin\phi(n)\sin\chi(n)$ and $x_3(n) = \rho(n)\cos\phi(n)$ where $x_i(n),\ i = 1, 2, 3$ are the received signals defined in (1). The joint pdf of the Cartesian tri-variate data in terms of its polar representation is then given by

$$p(x_1, x_2, x_3) = \frac{1}{|\mathbf{J}|}p\Big(\rho, \chi, \phi\Big), \tag{11}$$

such that $\rho = \sqrt{x_1^2 + x_2^2 + x_3^2}$, $\chi = \tan^{-1}\left(x_2/x_1\right)$ and $\phi = \tan^{-1}\left(x_3/\sqrt{x_1^2 + x_2^2}\right)$, where we have temporarily omitted the

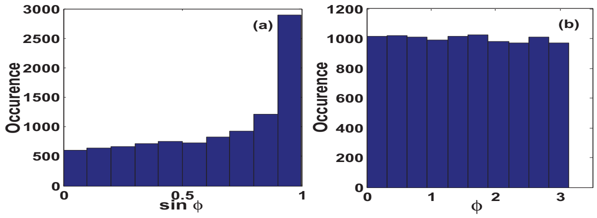

Fig. 3. Histogram plot of (a) $\sin\phi$ and (b) $\phi \sim \mathcal{U}(0,\pi)$.

time dependency '(n)' for compactness in notation and

$$|\mathbf{J}| = \begin{vmatrix} \sin\phi\cos\chi & -\rho\sin\phi\sin\chi & \rho\cos\phi\cos\chi \\ \sin\phi\sin\chi & \rho\sin\phi\cos\chi & \rho\cos\phi\sin\chi \\ \cos\phi & 0 & -\rho\sin\phi \end{vmatrix} = \rho^2\sin\phi \quad (12)$$

is the determinant of the Jacobian matrix $\mathbf{J}$. Substituting (9), (10) and (12) into (11), the pdf of the generalized Gaussian distribution is obtained as

$$\begin{aligned} p(x_1,x_2,x_3) &= \frac{1}{2\pi}\frac{1}{\pi}\frac{1}{\rho^2\sin\phi}\frac{k\rho^2}{\Gamma(3/k)}e^{-(x_1^2+x_2^2+x_3^2)^{k/2}} \\ &= \frac{c}{\pi^2\Gamma(3/2c)\sin\phi}e^{-(x_1^2+x_2^2+x_3^2)^c} \end{aligned} \quad (13)$$

where $c = k/2$. Figure 3(a) shows the distribution of $\sin\phi$ corresponding to a uniform distribution of elevation angle ϕ in Fig. 3(b) where we observe that $\sin\phi = 1$ occurs with the highest probability. With $\sin\phi \approx 1$ the generalized Gaussian pdf is reduced to

$$p(x_1,x_2,x_3) \approx ce^{-(x_1^2+x_2^2+x_3^2)^c}\Big/(\pi^2\Gamma(3/2c)). \quad (14)$$

For $c = 1$, the pdf $p(x_1,x_2,x_3)$ degenerates to a Gaussian distribution which is analogous to the CGGD for complex signals [6].

Since the three orthogonal sensors of the geophone are colocated, we assume that $E\{x_1^2\} = E\{x_2^2\} = E\{x_3^2\}$ and compute the second-order moment as

$$\begin{aligned} \xi(c) \triangleq E\{x_1^2\} &= \int_{-\infty}^{\infty}\int_{-\infty}^{\infty}\int_{-\infty}^{\infty} x_1^2 p(x_1,x_2,x_3)dx_1dx_2dx_3 \\ &= \int_0^{\pi}\int_0^{2\pi}\int_0^{\infty}\rho^2\sin^2\phi\cos^2\chi\frac{c\,e^{(\rho^2)^c}(\rho^2\sin\phi d\rho d\chi d\phi)}{\pi^2\Gamma(\frac{3}{2c})\sin\phi} \\ &= \frac{\Gamma(5/c)}{2\Gamma(3/2c)}. \end{aligned} \quad (15)$$

Similar to the approach in [6], we normalise the signal $x_i(n)$ with $\xi(c)$ to have unit variance using the linear transform $\mathbf{v}(n) = \mathbf{D}\mathbf{x}(n)$, where $\mathbf{D} = \sqrt{1/\xi(c)}\mathbf{I}_3$ and $\mathbf{I}_3$ is a 3×3 identity matrix. This transform is applied to (14) to obtain

$$p(\mathbf{v}) = \frac{1}{|\mathbf{D}|}p(\mathbf{D}^{-1}\mathbf{v}(n)) = \beta(c)e^{-\xi(c)[\mathbf{v}^T(n)\mathbf{v}(n)]^c}, \quad (16)$$

where $p(\mathbf{D}^{-1}\mathbf{v}(n)) = p(x_1,x_2,x_3)$, $\beta(c) = c\frac{\Gamma(5/c)}{(2\pi^2\Gamma(3/2c)^2)}$ and $E\{\mathbf{v}(n)\mathbf{v}^T(n)\} = \mathbf{I}_3$ for $c > 0$.

We express $\mathbf{v}(n)$ as an augmented quaternion vector $\mathfrak{q}_{\mathbf{v}}^{\mathrm{a}}(n)$ using (5) and the corresponding quaternion pdf is derived using (8) as

$$p(\mathfrak{q}_{\mathbf{v}}^{\mathrm{a}}) = \beta(c)e^{-\xi(c)[(\mathfrak{q}_{\mathbf{v}}^{\mathrm{a}})^H\mathfrak{q}_{\mathbf{v}}^{\mathrm{a}}]^c}. \quad (17)$$

In order to extend this pdf for any arbitrary quaternion augmented vector $\mathfrak{q}^{\mathrm{a}}$ with quaternion augmented covariance matrix $\mathbb{C}_{\mathfrak{q}}^{\mathrm{a}}$, we apply the transformation $\mathfrak{q}^{\mathrm{a}} = \mathbb{T}_{\mathfrak{q}}^{\mathrm{a}}\mathfrak{q}_{\mathbf{v}}^{\mathrm{a}}$, where $\mathbb{T}_{\mathfrak{q}}^{\mathrm{a}} = \sqrt{\mathbb{C}_{\mathfrak{q}}^{\mathrm{a}}}$. Since the diagonal elements of $\mathbb{C}_{\mathfrak{q}}^{\mathrm{a}}$ are real, we obtain the pdf of the QGGD as

$$p(\mathfrak{q}^{\mathrm{a}}) = \left(\sqrt{|\mathbb{C}_{\mathfrak{q}}^{\mathrm{a}}|}\right)^{-1}\beta(c)e^{-[\xi(c)((\mathfrak{q}^{\mathrm{a}})^H(\mathbb{C}_{\mathfrak{q}}^{\mathrm{a}})^{-1}\mathfrak{q}^{\mathrm{a}})]^c}, \quad (18)$$

where $\mathfrak{q}^{\mathrm{a}}$ and $\mathbb{C}_{\mathfrak{q}}^{\mathrm{a}}$ are defined similar to (5) and (6) respectively. The parameter c defines the shape of the vector-quaternion distribution while $\mathbb{C}_{\mathfrak{q}}^{\mathrm{a}}$ is the covariance matrix which preserves the inter-channel correlation between the orthogonal components of the vector-quaternion. We next fit overlapping frames of the vector-quaternion signal to the derived pdf and the presence of footsteps is detected through the estimation of c and $\mathbb{C}_{\mathfrak{q}}^{\mathrm{a}}$. The maximum likelihood estimates of these parameters derived using the QGGD pdf do not result in a closed form expression and hence we make use of numerical methods for their estimation.

4.1. Non-Gaussianity Measure

The shape of the vector-quaternion distribution, as illustrated in Fig. 1, is reflected in the c parameter of the QGGD in (18). It is estimated from the magnitude $\rho(n)$, which follows a GGaD pdf given in (9). A heuristic method [13] that maps the GGaD pdf to a Gamma distribution using the power transformation identity, i.e., when $\rho(n) \sim \mathrm{GGaD}(3/2c, 2c, 1)$ then $\rho^{2c}(n) \sim \mathrm{Gamma}(3/2c, 1^{2c})$, is used to estimate c. This routine iteratively loops through values of $\widehat{c} \in [0.1, 2]$ to estimate c as the best chi-square fit between $\rho^c(n)$ and an empirical Gamma distribution with the same parameters [13]. Thus $\widehat{c}$ is expected to be approximately equal to unity for Gaussian distributed noise and less than unity for super-Gaussian signal. Detection of footstep signals is therefore expressed as a binary hypothesis test using $\widehat{c}$ as

$$\begin{aligned} H_0 &: \widehat{c} \approx 1 \text{ for Gaussian noise} \\ H_1 &: \widehat{c} < 1 \text{ for Super} - \text{Gaussian footstep signal.} \end{aligned}$$

4.2. Improperness Measure

The augmented covariance matrix of the QGGD derived in (18) is estimated using a frame of N consecutive augmented quaternion vector defined using (5), as

$$\widehat{\mathbb{C}_{\mathfrak{q}}^{\mathrm{a}}} = \frac{1}{N}\sum_{n=0}^{N-1}\mathfrak{q}_{\mathrm{a}}(n)\mathfrak{q}_{\mathrm{a}}^H(n). \quad (19)$$

The estimated $\widehat{\mathbb{C}_{\mathfrak{q}}^{\mathrm{a}}}$ has a structure

$$\widehat{\mathbb{C}_{\mathfrak{q}}^{\mathrm{a}}} = \begin{bmatrix} \widehat{\mathbb{C}}_{\mathfrak{q}\mathfrak{q}} & \widehat{\mathbb{C}}_{\mathfrak{q}\mathfrak{q}^{\imath}} & \widehat{\mathbb{C}}_{\mathfrak{q}\mathfrak{q}^{\jmath}} & \widehat{\mathbb{C}}_{\mathfrak{q}\mathfrak{q}^{\kappa}} \\ \widehat{\mathbb{C}}_{\mathfrak{q}^{\imath}\mathfrak{q}} & \widehat{\mathbb{C}}_{\mathfrak{q}^{\imath}\mathfrak{q}^{\imath}} & \widehat{\mathbb{C}}_{\mathfrak{q}^{\imath}\mathfrak{q}^{\jmath}} & \widehat{\mathbb{C}}_{\mathfrak{q}^{\imath}\mathfrak{q}^{\kappa}} \\ \widehat{\mathbb{C}}_{\mathfrak{q}^{\jmath}\mathfrak{q}} & \widehat{\mathbb{C}}_{\mathfrak{q}^{\jmath}\mathfrak{q}^{\imath}} & \widehat{\mathbb{C}}_{\mathfrak{q}^{\jmath}\mathfrak{q}^{\jmath}} & \widehat{\mathbb{C}}_{\mathfrak{q}^{\jmath}\mathfrak{q}^{\kappa}} \\ \widehat{\mathbb{C}}_{\mathfrak{q}^{\kappa}\mathfrak{q}} & \widehat{\mathbb{C}}_{\mathfrak{q}^{\kappa}\mathfrak{q}^{\imath}} & \widehat{\mathbb{C}}_{\mathfrak{q}^{\kappa}\mathfrak{q}^{\jmath}} & \widehat{\mathbb{C}}_{\mathfrak{q}^{\kappa}\mathfrak{q}^{\kappa}} \end{bmatrix}, \quad (20)$$

where the off-diagonal elements are the pseudo-covariances

$$\widehat{\mathbb{C}}_{\mathfrak{q}\mathfrak{q}^{\imath}} = \frac{1}{N}\sum_{n=0}^{N-1}q(n)(q^{\imath})^H(n). \quad (21)$$

The augmented covariance matrix quantifies the correlation between the orthogonal axes of the geophone which is dependent on the signal power. The matrix $\widehat{\mathbb{C}_{\mathfrak{q}}^{\mathrm{a}}}$ is $\mathbb{Q}$-proper if and only if the pseudo-covariances with respect to $\imath$, $\jmath$ and κ vanish and $\mathbb{Q}$-improper if none

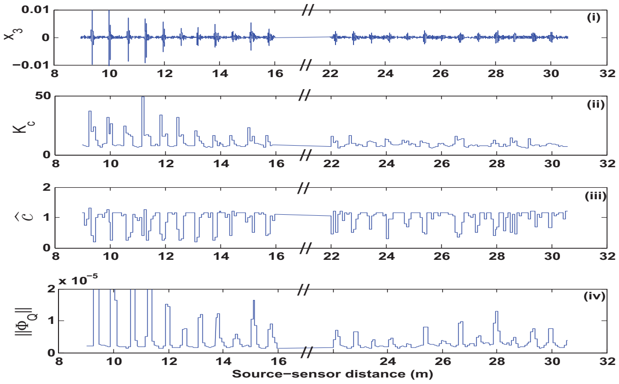

Fig. 4. Plot of (i) z-axis signal, (ii) cumulative kurtosis $K_{\rm c}$, (iii) shape parameter $\widehat{c}$ and (iv) $||\Phi_{\mathbb{Q}}||$, for radial walk from 9 m to 30 m.

of them vanish [14, 15]. Random Gaussian noise with comparable power in all the three channels of the geophone results in an unpolarized $\mathbb{Q}$-proper diagonal structure since there exists no correlation between the orthogonal axes. However, as seen in Fig. 2(b), footstep signals are expected to be $\mathbb{Q}$-improper due to the presence of elliptically polarized signals and the amount of correlation is described using the degree-of-$\mathbb{Q}$-improperness (DOI). The locally most powerful invariant test [16] is used to quantify the DOI and is defined as the Frobenius norm $||\Phi_{\mathbb{Q}}||$ of the $\mathbb{Q}$-coherence matrix

$$\Phi_{\mathbb{Q}} = (\widetilde{\mathbb{C}^{\rm a}_{\rm q}})^{-1/2}\widehat{\mathbb{C}^{\rm a}_{\rm q}}(\widetilde{\mathbb{C}^{\rm a}_{\rm q}})^{-1/2}, \tag{22}$$

where $\widehat{\mathbb{C}^{\rm a}_{\rm q}}$ is the estimated augmented matrix and $\widetilde{\mathbb{C}^{\rm a}_{\rm q}}$ is the augmented matrix with a $\mathbb{Q}$-proper diagonal structure.

In practical scenarios, perfectly unpolarized $\mathbb{Q}$-proper signals are difficult to obtain due to the presence of standing waves, earth vibrations in the distant environment and differences in the channel gain [9]. In this work we define $\widetilde{\mathbb{C}^{\rm a}_{\rm q}} = \mathbf{I}_4$ to evaluate $||\Phi_{\mathbb{Q}}||$ by preserving the energy of the vector-quaternion signal. The evaluated $||\Phi_{\mathbb{Q}}||$ is expected to be high in the presence of a polarized footstep and low in the absence of it. Footstep detection can therefore be defined as a binary hypothesis test using DOI as

$$\begin{aligned} H_0 \quad &: \quad ||\Phi_{\mathbb{Q}}|| < \gamma \text{ for } \mathbb{Q}\text{−Proper noise} \\ H_1 \quad &: \quad ||\Phi_{\mathbb{Q}}|| > \gamma \text{ for } \mathbb{Q}\text{−Improper footstep signal}, \end{aligned} \tag{23}$$

where γ is a threshold. Since footsteps are intermittent and impulsive, the noise statistics is estimated by evaluating the DOI metric over long-time window, denoted as $\rm DOI_n$. An adaptive detection threshold is evaluated as

$$\gamma(l) = \eta \times \mathrm{DOI_n}, \tag{24}$$

where the scaling parameter $\eta > 0$ regulates the trade-off between the probability of detection and false alarm.

5. EXPERIMENTAL RESULTS

We analyse the performance of the proposed metrics on footsteps recorded by a tri-axial geophone for a person walking radially away from the sensor from 2 m to 30 m and for a person marching at fixed distance of 11 m from the sensor. These experiments evaluate the robustness of the metrics under practical conditions of increasing source-sensor distances and presence of standing waves. Experiments were conducted on a grassy field with a single person walking with hard sole shoes. The proposed metrics $\widehat{c}$ and $||\Phi_{\mathbb{Q}}||$ are compared with cumulative kurtosis $K_{\rm c}$, which is evaluated as the sum

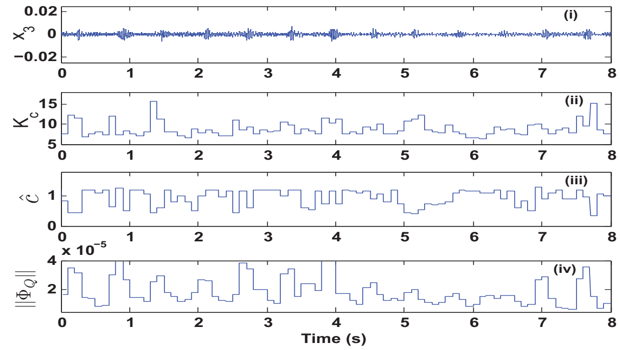

Fig. 5. Plot of (i) z-axis signal, (ii) $K_{\rm c}$, (iii) shape parameter $\widehat{c}$ and (iv) $||\Phi_{\mathbb{Q}}||$, for stationary footsteps at 11 m from sensor.

of kurtosis of the three-channel data [9]. The metrics are evaluated using a sliding window of length 200 ms with 50% overlap on data resampled to 8 kHz.

Figure 4(i) shows the signal acquired by the x_3-component of the geophone for the radial-walk experiment. As the source moves away from the sensor the leptokurtic nature of the footstep impulse reduces owing to longer propagation in the medium. This directly reflects in the deterioration of the detection performance of $K_{\rm c}$ illustrated in Fig. 4(ii), especially for source-sensor distances greater than 25 m. Although the estimated $\widehat{c}$ plotted in Fig. 4(iii) quantifies the super-Gaussianity of the signal, it shows superior distinction of footstep segments than $K_{\rm c}$ at farther source-sensor distances. The DOI metric $||\Phi_{\mathbb{Q}}||$ plotted in Fig. 4(iv) shows consistent detection of footsteps at farther distances and does not show any spurious peaks as the value of the metric corresponding to footstep segment is distinctly higher to that of noise.

Figure 5 plots the detection metrics for stationary footsteps in the presence of a bus in the background. The existence of standing waves along with increased noise level results in the spread of the source impulse. This causes inconsistency in both $K_{\rm c}$ and $\widehat{c}$ whereas the corresponding DOI metric is consistent even in the presence of noise. We define detection rate $\rm R_d$ and false alarm rate $\rm R_{fa}$ as

$$\mathrm{R_d} = \frac{\text{no. of footsteps detected}}{\text{total no. of footsteps}}, \mathrm{R_{fa}} = \frac{\text{no. of false detections}}{\text{total no. of footsteps}}. \tag{25}$$

The detection performance averaged over thirty experiments involving random, radial and zig-zag walk with $\eta = 0.98$ for $||\Phi_{\mathbb{Q}}||$ is compared in Table 1. From the results, we note that the DOI metric $||\Phi_{\mathbb{Q}}||$ outperforms $K_{\rm c}$ and $\widehat{c}$ with improved detection of footsteps at farther source-sensor distances for both walking patterns.

Table 1. Comparison of Detection Performance

Walking Style	Distance	$K_{\rm c}$		$\lVert\Phi_{\mathbb{Q}}\rVert$		$\widehat{c}$	
		$R_{\rm d}$	$R_{\rm fa}$	$R_{\rm d}$	$R_{\rm fa}$	$R_{\rm d}$	$R_{\rm fa}$
Stationary Marching	$<$ 10 m	0.99	0.005	0.98	0.005	0.93	0.2
	10-20 m	0.7	0.06	0.95	0.08	0.8	0.17
Radial Walking	$<$ 10 m	1	0	1	0	1	0
	10-30 m	0.9	0.1	0.94	0.02	0.8	0.15

6. CONCLUSION

The QGGD was derived to statistically define the diversity in the vector-quaternion signal using a shape parameter and quaternion augmented covariance matrix and used for footstep detection. We show that the degree-of-$\mathbb{Q}$-improperness effectively quantifies the correlation in the tri-axial data and thus performs better than the metrics based on the shape of the signal distribution.

7. REFERENCES

[1] G. Succi, D. Clapp, R. Gampert, and G. Prado, "Footstep detection and tracking," *in Proc. SPIE*, vol. 4393, pp. 22–29, 2001.

[2] G. Miller and H. Pursey, "On the partition of energy between elastic waves in a semi-infinite solid," *Proc. Royal Society London, Series A*, vol. 233, pp. 55–69, 1955.

[3] N. L. Bihan and J. Mars, "Singular value decomposition of quaternion matrices: a new tool for vector-sensor signal processing," *Signal Process.*, vol. 84, no. 7, pp. 1177–1199, 2004.

[4] S. Anderson and A. Nehorai, "Analysis of a polarised seismic wave model," *IEEE Trans. Signal Process.*, vol. 44, pp. 379–386, 1996.

[5] N. L. Bihan and P.-O. Amblard, "Detection and estimation of Gaussian proper quaternion valued random processes," in *Proc. IMA Conf. on Mathematics*, 2006.

[6] M. Novey, T. Adali, and A. Roy, "A complex generalized Gaussian distribution characterization, generation, and estimation," *IEEE Trans. Signal Process.*, vol. 58, pp. 1427–1433, 2010.

[7] M. Novey, T. Adali, and A. Roy, "Circularity and gaussianity detection using the complex generalized gaussian distribution," *IEEE Signal Process. Letters*, vol. 16, pp. 993–996, 2009.

[8] K. Wong and M. Zoltowski, "Orthogonal velocity-hydrophone ESPRIT for sonar source localization," *Proc. IEEE Conf. on 'Prospects for the 21st Century'*, pp. 1307–1312, 1996.

[9] D. Venkatraman, V. Reddy, A. W. H. Khong, and B. P. Ng, "Polarization-cum-energy metric for footstep detection using vector-sensor," in *Proc. IEEE Intl. Conf. on Technologies for Homeland Security*, Nov 2011.

[10] S. Greenhalgh, I. Mason, and B. Zhou, "An analytical treatment of single station triaxial seismic direction finding," *Journal of Geophysics and Engineering*, vol. 2, pp. 8–15, 1995.

[11] C. C. Took and D. P. Mandic, "Augmented second-order statistics of quaternion random signals," *Signal Process.*, vol. 91, no. 2, pp. 214 – 224, 2011.

[12] M. Khodabin and A. Ahmadabadi, "Some properties of generalized Gamma distribution," *Mathematical Sciences*, vol. 4, pp. 9–28, 2010.

[13] O. Gomes, C. Combes, and A. Dussauchoy, "Parameter estimation of the generalized Gamma distribution," *Mathematics and Computers in Simulation*, vol. 79, no. 4, pp. 955–963, 2008.

[14] P. Ginzberg and A. Walden, "Testing for quaternion propriety," *IEEE Trans. Signal Process.*, vol. 59, no. 7, pp. 3025 –3034, Jul 2011.

[15] J. Via, D. Palomar, and L. Vielva, "Generalized likelihood ratios for testing the properness of quaternion Gaussian vectors," *IEEE Trans. Signal Process.*, vol. 59, no. 4, pp. 1356 –1370, April 2011.

[16] J. Via and L. Vielva, "Locally most powerful invariant tests for the properness of quaternion Gaussian vectors," *IEEE Trans. Signal Process.*, vol. 60, no. 3, pp. 997 – 1009, 2012.